Unsteady flow of silica nanofluid over a stretching cylinder with effects of different shapes of nanoparticles and Joule heating

Ramzan Ali[a]*, Azhar Iqbal[b], Tasawar Abbass[b], Touqeer Arshad[c], Azeem Shahzad[d]

[a]University of Doha for Science and Technology, College of General Education, Department of Mathematics, Doha, Qatar
[b]Department of Mathematics, University of Wah, Wah Cantt, 47040, Pakistan.
[c]Department of Basic Sciences, University of Engineering and Technology, Taxila,47050, Pakistan.
[d]Department of Mathematical Sciences, University of Engineering and Technology, Taxila,47050, Pakistan.
*Corresponding author email: ramzan.ali@udst.edu.qa

Abstract

Indeed, nanofluids have garnered significant interest in various fields due to their numerous advantages and potential applications. The appeal of SiO_2 nanofluid, in particular, lies in its low preparation cost, simple production process, controlled chemistry, environmental safety and its exceptional ability to be homogeneously suspended in the base fluid, which makes it a promising candidate for a variety of applications. In this study, we investigate the flow analysis of a water based silicon dioxide nanofluid, passing over a stretched cylinder while subjected to a continuous magnetic field, including Joule heating effects. The research involves the development of a mathematical model and the formulation of governing equations represented as partial differential equations. These equations are subsequently transformed into non-linear ordinary differential equations through suitable transformations. To obtain a numerical solution, the MATLAB bvp4c solver technique is employed. The study investigates the implications of dimensionless parameters on velocity and thermal distributions. It is observed that the velocity distribution $f'(\eta)$ exhibits a direct relationship with the volumetric fraction ϕ and an inverse relationship with the unsteadiness parameter S, the magnetic parameter M, and the temperature distribution $\theta(\eta)$ shows an enhancement for the increasing ϕ and M, as well as the Eckert number. However, it declines against S and the Prandtl number. The results for local Nusselt number and skin frictions are depicted in Tables.

Keywords: Joule heating; MHD flow; SiO_2-H_2O nanofluid

1. Introduction

Nanotechnology is the practice of manipulating matter at the atomic, molecular and supramolecular levels. It encompasses the design and construction of materials, electronics, and structures with dimensions ranging from 1–100 nm. Nanotechnology finds application in diverse fields, such as environmental research, medicine, materials science, energy, and electronics. By working on such a minute scale, nanotechnology opens up new possibilities and potential advancements in various industries and scientific disciplines. Nanofluids refer to colloidal suspensions of nanoparticles within a base fluid. These nanoparticles vary in size from one to one hundred nanometers and can consist of diverse materials, including metals, oxides, carbides, and carbon nanotubes. The base fluid can be water, oil or another type of liquid. The concept of nanofluids was first proposed in the early 1990s [1], and since then, extensive research has been conducted to explore their potential applications in heat transfer. The incorporation of nanoparticles in a nanofluid significantly enhances the thermal conductivity of the base fluid, leading to

Nomenclature

A – proportionality constant
B – magnetic field
b – dimensional constant
Ec – Eckert number
$f'(\eta)$ – dimensionless velocity distribution
K – slip parameter
m – shape factor
Nu – Nusselt number
Pr – Prandtl number
p – pressure
Re – Reynolds number
S – unsteadiness parameter
T – temperature, K
t – time, s
U – surface velocity, m/s

Greek symbols

α, α_1 – dimensional constants
η – similarity variable
$\theta(\eta)$ – dimensionless temperature distribution
v – kinematic viscosity, m^2/s
μ – dynamic viscosity, Pa·s
ρ – density, kg/m^3
σ – electrical conductivity, S/m
ϕ – volumetric fraction of nanoparticles

Subscripts and Superscripts

f – fluid
nf – nanofluid
s – solid particles

Abbreviations and Acronyms

MHD – magnetohydrodynamics
ODEs – ordinary differential equations
PDEs – partial differential equations

improved heat transfer performance across a wide range of applications such as electronic cooling, using the thermophysical properties of SiO_2 in fuel cell [2], in a lithium ion battery, in the presence of phase change material [3]. Akram et al. [4] studied ethylene glycol based nanofluid for electroosmotic and peristaltic pumping, other authors employed similar nanofluidic models in solar heating systems [5,6], and Ma et al. [7] extended the models for nuclear power plants. Arif et al. [8] studied a fractional model of coupled stress Casson tri-hybrid nano-fluid using dissimilar shape nanoparticles. A mathematical simulations framework is proposed by Akram et al. [9] for peristaltic pumping of nanofluid due to induced magnetic field in a non-uniform channel.

A boundary layer refers to a slender layer of fluid that forms as the fluid flows adjacent to a solid surface. Various engineering disciplines, such as aerodynamics, heat transport and fluid mechanics, extensively depend on the understanding of boundary layer flow. This phenomenon plays a crucial role in generating drag force experienced by objects moving through a fluid, as well as facilitating the exchange of heat and mass between the fluid and the solid item. In 1970, Crane [10] conducted pioneering research on boundary layer flow over a stretching surface. He developed a mathematical model to describe the two-dimensional incompressible flow of a Newtonian fluid within the boundary layer. To solve this model, Crane utilized similarity transformations, a powerful mathematical technique commonly employed in fluid mechanics. Researchers have explored and analyzed the flow behaviour for diverse shapes and arrangements, contributing to a comprehensive understanding of this fundamental fluid mechanics phenomenon.

Ahmed et al. [11] proposed a framework of non-Newtonian fluid model of Jeffrey type over a stretching sheet for a convective heat transfer. Meanwhile, Hayat et al. [12] provided a numerical simulation for heat enhancement using copper nanoparticles dispersed in ethylene glycol, and furthermore studied similar models for diverse geometrical effects [13], and for the axisymmetric stagnation point flow [14] over an unsteady radial surface, the Casson fluid for convective squeeze flow [15].

Jabeen et al. [16] studied numerically Williamson nanofluid in the presence of viscous dissipation for bioconvection and energy activation and the case of inclined stretching cylinder was considered by Othman et al. [17]. In a series of articles, Hayat et al. [18] provided a comparative study of thin film flow for wide range of nanofluidic particles in stretchable surfaces [19] using boundary layer flows [20].

The study of Joule heating in nanofluids is a relatively recent area of research that began in the early 2000s with initial investigations into this phenomenon. Subsequently, there has been a notable increase in research efforts aimed at comprehending the effects of Joule heating on nanofluids. This extensive exploration has demonstrated that Joule heating has a significant impact on the performance of nanofluids, highlighting its importance as a critical factor to be taken into account in various nanofluid-related applications and systems. The effects of Joule heating are determined by the product of the magnetic parameter and the Eckert number. Numerous studies have been conducted to investigate the impact of Joule heating in magnetohydrodynamic (MHD) channels under various conditions. This research aims to understand the influence of Joule heating on fluid flow, heat transfer, and other relevant phenomena in MHD systems. Chen [21] explored the combined heat and mass transfer in buoyancy-induced MHD natural convection flow of an electrically conducting fluid down a vertical plate. Ohmic and viscous heating effects are taken into account. Cao et al. [22] provided an overview of the use of electrohydrodynamics and Joule heating effects of direct current (DC) and alternating current (AC) in microfluidic chips. Hayat et al. [23] analyzed MHD flow of Cu–water nanofluid over a stretched sheet. Joule heating and viscous dissipation effects are also studied in this article. Maraj et al. [24] examined effects of joule heating, partial slip and viscous dissipation on an electrically conducting Casson nanofluid flow, as well as heat and mass transfer, over a nonlinearly stretched horizontal sheet. For Khashi'ie et al. [25] the main objectives of the study are to achieve the duality of solutions and investigate the flow and heat transfer characteristics of the hybrid nanofluid while it passes over a shrinking cylinder with the inf-

luence of Joule heating. Naseem et al. [26] are considering an MHDs boundary layer flow past a flat plate with the inclusion of variable temperature, radiation, Joule heating and viscous dissipation effects. Rehman et al. [27] investigates the characteristics of the melting heat phenomenon in a Powell-Eyring fluid flow deformed by a linearly stretchable sheet near the stagnation point. To disclose the heat transport properties, the study incorporates quadratic thermal stratification, thermal radiation, viscous dissipation and Joule heating. Investigation of the unsteady stagnation-point flow performance of a TiO_2-$C_2H_6O_2$ nanofluid around a shrinking horizontal cylinder is carried out by Makhdoum et al. [28]. The research takes into consideration various influencing factors such as a magnetic field, Joule heating, viscous dissipation, nanoparticles aggregation and mass suction. These elements are studied to understand their effects on the boundary layer flow characteristics of the nanofluid. Raza et al. [29] accomplished analysis of a radiative Sutterby nanofluid flow containing suspended swimming microorganisms over a stretchable cylinder. The article extensively explored the effects of Brownian motion, thermophoresis, Joule heating and viscous dissipation in the presence of stratification parameters. Alsaedi et al. [30] described the bioconvective flow of Reiner-Rivlin liquid susceptible to motile microorganisms.

Wazawa and Nagai [31] analyzed and characterized several parameters in Joule heating due to ion currents through proteins channel, and Manshadi and Beskok [32] extended the idea of Joule heating induced transport in microchannels. In addition, Khan et al. [33] and Narayanaswamy et al. [34] provided a new framework on suppression of heat transfer in vertical tube through suspension of alumina nanoparticles using Joule heating and thermal radiations [35].

The peculiarity of this study lies in its examination of the unsteady flow of nanofluid around a stretchable cylinder. Additionally, the study investigates the influence of different shapes of SiO_2 nanoparticles on the nanofluid's flow behaviour and heat transfer, particularly with consideration of the Joule heating effect. In this study, the impact of relevant factors on the flow and temperature is graphically analyzed. Charts are employed to present the computational results of skin friction coefficient and heat transfer rate. The main findings are systematically organized and summarized in the conclusions section.

2. Physical and mathematical description of the problem

In this particular problem, the stretching of a cylinder with surface velocity along the z-axis

$$U(z,t) = \frac{bz}{1-\alpha_1 t}$$

induces an unsteady three-dimensional (3D) flow of nanofluid, as illustrated in Fig. 1. The temperature field is denoted by

$$T_s(z,t) = T_0 - T_r \frac{bz^2}{2v_f}(1-\alpha_1 t)^{-3/2},$$

with α_1 and b representing dimensional constants. Here, T_r is the reference temperature, T_0 is the ambient temperature, and v_f is the kinematic viscosity of the base fluid. Additionally, a uniform magnetic field

$$B(t) = \frac{B_0}{(1-\alpha_1 t)^{1/2}},$$

is considered to act along the radial axis.
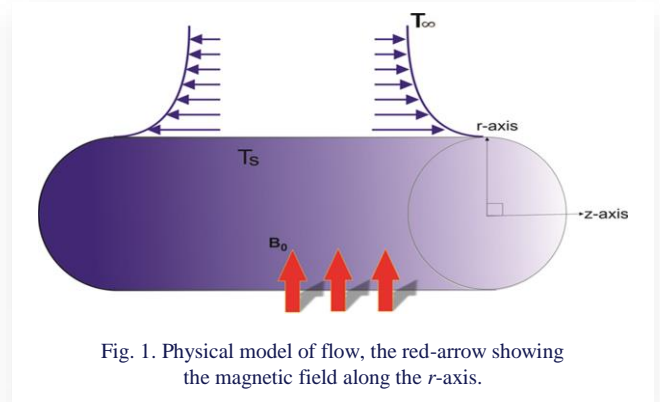
Fig. 1. Physical model of flow, the red-arrow showing the magnetic field along the r-axis.

According to the usual notation, governing equation of continuity, momentum, and thermal energy for the current study are expressed as follows:

$$\frac{\partial}{\partial r(ru)} + \frac{\partial}{\partial z(rw)} = 0, \tag{1}$$

$$\frac{\partial w}{\partial t} + u\frac{\partial w}{\partial r} + w\frac{\partial w}{\partial z} = \frac{v_{nf}}{r}\frac{\partial}{\partial r}\left(r\frac{\partial w}{\partial r}\right) - w\frac{\sigma_{nf}}{\rho_{nf}}\cdot\frac{B_0^2}{(1-\alpha_1 t)}, \tag{2}$$

$$\frac{\partial T}{\partial t} + u\frac{\partial T}{\partial r} + w\frac{\partial T}{\partial z} = \frac{\mu_{nf}}{\rho_{nf}C_p}\left(\frac{\partial w}{\partial r}\right)^2 + \alpha_{nf}\left[\frac{\partial^2 T}{\partial r^2} + \frac{1}{r}\left(\frac{\partial T}{\partial r}\right)\right] + \frac{\sigma_{nf}B_0^2}{[(\rho C)_p]_{nf}}w^2. \tag{3}$$

Equations (1)–(3) are subjected to the boundary conditions

- at $r = R$: $\quad w = U_w + Av_f\frac{\partial w}{\partial r}, \quad u = 0, \quad T_s = T$

- as $r \to \infty$: $\quad w \to 0, \quad T \to T_0$. (4)

Thermo-physical properties in Eqs. (1)–(4) are defined in Table 1.

Table 1. Thermophysical properties of nanofluid. [36, 37].

Properties	Mathematical form
Kinematic viscosity	$v_{nf} = \frac{\mu_{nf}}{\rho_{nf}},$
Dynamic viscosity	$\mu_{nf} = \mu_f(1 + A_1\phi + A_2\phi^2)$
Electrical conductivity	$\sigma_{nf} = \sigma_f(1-\phi) + \phi\sigma_s$
Density	$\rho_{nf} = (1-\phi)\rho_f + \phi\rho_s$,
Heat capacity	$(\rho C_p)_{nf} = (1-\phi)(\rho C_p)_f + \phi(\rho C_p)_s,$
Diffusivity	$\alpha_{nf} = \frac{k_{nf}}{(\rho C_p)_{nf}},$
Thermal conductivity	$\frac{k_{nf}}{k_f} = \left[\frac{k_s + (m-1)k_f + (m-1)(k_s-k_f)\phi}{k_s + (m-1)k_f - (k_s-k_f)\phi}\right].$

In addition to the previously mentioned parameters, the equation involves the following coefficients and constants:
- A_1: viscosity enhancement coefficient,
- A_2: heat capacitance coefficient,
- h_f: convective heat transfer constant,
- A: proportionality constant,
- ϕ: volume fraction of SiO_2 in the nanofluid.

These coefficients and constants play crucial roles in determining the behaviour of the nanofluid flow and heat transfer, particularly in relation to the viscosity, heat capacitance, convective heat transfer and the influence of SiO_2 nanoparticles' volume fraction. Table 2 shows the values of the viscosity enhancement coefficient (A_1), heat capacitance coefficient (A_2) and form factors. Table 3 shows the thermo-physical characteristics of the fluid and silica.

Table 2. Impact of incipient factors on skin friction $-f''(0)$.

Ø	S	K	Ec	M	Pr	Sphere	Blade	Cylinder	Platelets
0.02	0.2	0.5	0.5	0.5	6.0	0.80163391	0.9346161	1.1070321	1.2776538
0.04	-	-	-	-	-	0.83543901	1.091834	1.7184747	1.9118712
0.06	-	-	-	-	-	0.87173587	1.2441354	2.5194769	2.64974
0.08		-	-	-	-	0.91043654	1.3928966	3.4801488	3.4868193
0.02	0.0	-	-	-	-	0.77531893	0.90361498	1.0700079	1.2347688
-	0.2	-	-	-	-	0.80163391	0.9346161	1.1070321	1.2776538
-	0.4	-	-	-	-	0.82600329	0.96339731	1.1415057	1.3176906
-	0.6	-	-	-	-	0.84861013	0.99016497	1.1736609	1.3551333
-	0.2	0.5	-	-	-	0.80163391	0.9346161	1.1070321	1.2776538
-	-	1.0	-	-	-	0.5654237	0.66873311	0.80475493	0.94130412
-	-	1.5	-	-	-	0.43972782	0.52414435	0.63632519	0.74994213
-	-	2.0	-	-	-	0.36083911	0.4322793	0.52780859	0.62514519
-	-	0.5	0.0	-	-	0.8016338	0.93461598	1.1070319	1.2776536
-	-	-	0.5	-	-	0.80163391	0.9346161	1.1070321	1.2776538
-	-	-	1.0	-	-	0.80163413	0.93461635	1.1070324	1.2776541
-	-	-	1.5	-	-	0.8016346	0.93461789	1.107034	1.2776558
-	-	-	0.5	0.0	-	0.70500522	0.82146064	0.97286742	1.1232813
-	-	-	-	0.5	-	0.80163391	0.9346161	1.1070321	1.2776538
-	-	-	-	1.0	-	0.87293338	1.0190793	1.2085495	1.3959192
-	-	-	-	1.5	-	0.92945001	1.0865073	1.2902392	1.4917594
-	-	-	-	0.5	4.0	0.8016346	0.93461788	1.107034	1.2776557
-	-	-	-	-	6.0	0.80163391	0.9346161	1.1070321	1.2776538
-	-	-	-	-	8.0	0.80163374	0.93461591	1.1070319	1.2776536
-	-	-	-	-	10.0	0.80163371	0.93461588	1.1070319	1.2776535

Table 3. Impact of emerging parameters on local Nusselt number $-\theta'(0)$.

Ø	S	K	Ec	M	Pr	Sphere	Blade	Cylinder	Platelets
0.02	0.2	0.5	0.5	0.5	6.0	2.9465264	2.9790597	3.0000152	3.0117782
0.04	-	-	-	-	-	2.961509	3.0129846	3.0235016	3.0148118
0.06	-	-	-	-	-	2.9761148	3.0383966	2.9788285	2.9663797
0.08		-	-	-	-	2.9902525	3.0580802	2.8791404	2.8805444
0.02	0.0	-	-	-	-	2.7168342	2.755958	2.78315	2.7987929
-	0.2	-	-	-	-	2.9465264	2.9790597	3.0000152	3.0117782
-	0.4	-	-	-	-	3.162634	3.1899354	3.2055882	3.2138224
-	0.6	-	-	-	-	3.3671808	3.3902631	3.4014138	3.406517
-	0.2	0.5	-	-	-	2.9465264	2.9790597	3.0000152	3.0117782
-	-	1.0	-	-	-	2.7083412	2.7588335	2.8024725	2.8350076
-	-	1.5	-	-	-	2.5314231	2.5880426	2.6408211	2.6826098
-	-	2.0	-	-	-	2.3972012	2.4554346	2.5117424	2.557684
-	-	0.5	0.0	-	-	3.1842384	3.2548878	3.3231226	3.3800661
-	-	-	0.5	-	-	2.9465264	2.9790597	3.0000152	3.0117782
-	-	-	1.0	-	-	2.7088149	2.7032319	2.6769078	2.6434903
-	-	-	1.5	-	-	2.4711049	2.427418	2.3538109	2.2752103
-	-	-	0.5	0.0	-	3.0451521	3.0664606	3.075619	3.0781856
-	-	-	-	0.5	-	2.9465264	2.9790597	3.0000152	3.0117782
-	-	-	-	1.0	-	2.864198	2.9050168	2.9347271	2.9532537
-	-	-	-	1.5	-	2.7932117	2.8406537	2.877529	2.9016253
-	-	-	-	0.5	4.0	2.4022243	2.4339983	2.4567606	2.4710008
-	-	-	-	-	6.0	2.9465264	2.9790597	3.0000152	3.0117782
-	-	-	-	-	8.0	3.4030649	3.4360023	3.4552401	3.4647965
-	-	-	-	-	10.0	3.8038222	3.8370168	3.8546711	3.862244

$$\Psi = (Uvz)^{1/2} Rf(\eta), \qquad (5a)$$

$$\eta = \frac{r^2 - R^2}{2R} \left(\frac{U}{vz}\right)^{1/2} \qquad (5b)$$

$$\theta(\eta) = \frac{T - T_o}{-T_r \left[\frac{bz^2}{2v}\right][1 - \alpha_1 t]^{-3/2}}. \qquad (5c)$$

In this context, Ψ represents the stream function, while u and w denote the velocity components that satisfy the continuity

equation. The velocity components can be expressed as follows:

$$u = \frac{-1}{r}\frac{\partial \Psi}{\partial z} = \frac{-R}{r}\left(\frac{bv}{1-\alpha_1 t}\right)^{1/2} f(\eta), \qquad (6a)$$

$$w = \frac{1}{r}\frac{\partial \Psi}{\partial r} = \frac{bz}{(1-\alpha_1 t)}f'. \qquad (6b)$$

Here, u and w are the axial and radial velocity components, respectively, and they are related to the stream function Ψ in such a way that the continuity Eq. (1) remains satisfied.

So by using Eq. (5) and Eq. (6) we have:

$$[1 + 2C\eta]\epsilon_1 f''' + 2C\epsilon_1 f'' - [\epsilon_3 M + S]f' - \frac{\eta}{2}Sf'' +$$
$$+ff'' - (f')^2 = 0, \qquad (7)$$

$$[1 + 2C\eta]\theta'' + 2C\theta' + \frac{\Pr}{\epsilon_2}[f\theta' - 2f'\theta - \frac{s}{2}(3\theta + \eta\theta') +$$
$$+\text{Ec}\,\epsilon_1(1 + 2C\eta)(f'')^2] + \frac{\epsilon_1 M\,\text{Ec}\,\Pr}{\epsilon_2}(f')^2 = 0, \qquad (8)$$

and boundary conditions are:

$$f'(\infty) = 0, \qquad f'(0) = 1 + kf''(0),$$
$$\theta(0) = 1, \qquad \theta(\infty) = 0, \qquad (9)$$

where the Eckert number, curvature parameter, Prandtl number, unsteadiness parameter, magnetic parameter and slip parameter, respectively, are defined as:

$$\text{Ec} = \frac{U^2}{C_p \Delta T}, \qquad C = \sqrt{\frac{(1-\alpha_1 t)v_f}{bR^2}}, \qquad \Pr = \frac{v_f(\rho C_p)_f}{K_f},$$

$$S = \frac{\alpha_1}{b}, \qquad M = \frac{\sigma_f B_0^2}{\rho_f b}, \qquad K = A\left[\frac{v_f U_w}{z}\right]^{1/2},$$

where

$$\epsilon_1 = \frac{1+\phi A_1+\phi^2 A_2}{1-\phi+\phi\left(\frac{\rho_s}{\rho_f}\right)}, \qquad \epsilon_2 = \frac{\frac{k_{nf}}{k_f}}{1-\phi+\frac{\phi(\rho C_p)_s}{(\rho C_p)_f}}, \qquad (10a)$$

$$\epsilon_3 = \frac{1-\phi+\phi\left(\frac{\sigma_s}{\sigma_f}\right)}{1-\phi+\phi\left(\frac{\rho_s}{\rho_f}\right)}, \qquad \epsilon_4 = \frac{1-\phi+\phi\left(\frac{\sigma_s}{\sigma_f}\right)}{1-\phi+\frac{\phi(\rho C_p)_s}{(\rho C_p)_f}}, \qquad (10b)$$

where ϵ_i, $i = 1, 2, 3, 4$, are constants.

The values of Cf and Nu provide valuable insights into the flow and heat transfer characteristics of the nanofluid around the cylinder, and are defined as:

$$Cf = \frac{T_w}{\rho_f U_w^2}, \qquad \text{with} \qquad T_w = \mu_{nf}\left[\frac{\partial w}{\partial r}\right]_{r=R},$$

$$\text{Nu} = \frac{rq_w}{K_f(T_s-T_o)}, \qquad \text{with} \qquad q_w = -K_{nf}\left[\frac{\partial T}{\partial r}\right]_{r=R}.$$

They take the dimensionless form as:

$$\text{Re}^{\frac{1}{2}}C_f = (1 + \phi A_1 + \phi^2 A_2)f''(0), \qquad (11)$$

and

$$\text{Re}^{\frac{-1}{2}}N_u = -\frac{k_{nf}}{k_f}\theta'(0), \qquad (12)$$

where the Reynolds number is defined as $\text{Re} = \frac{Uz}{v}$.

3. Numerical procedure

The renowned and efficient BVP4C method in MATLAB is employed to numerically solve the reduced nonlinear system of ordinary differential equations (ODEs) (7) and (8) along with the given boundary conditions (BC) (9). To facilitate the numerical solution, these nonlinear ODEs are converted into a system of first-order ODEs, and the boundary conditions are substituted with appropriate initial conditions by tagging the variables as such:

$$(f, f' = y_1', f'' = y_2', \theta, y_4' = \theta') = (y_1, y_2, y_3, y_4, y_5),$$

so Eqs. (7) and (8) in program's algorithm take the form:

$$f''' = \frac{1}{\epsilon_1(1+2Ct)}\left(-2\epsilon_1 Cy(3) + (\epsilon_3 M + S)y(2) + \right.$$
$$\left. + \frac{S\eta y(3)}{2} - y(1)y(3) + y(2)^2\right),$$

and

$$\theta'' = \frac{1}{1+2\eta C}\left(-2Cy(5) - \frac{\Pr}{\epsilon_2}(y(1)y(5) - 2y(2)y(4) - \right.$$
$$+\frac{s}{2}(3y(4) + \eta y(5)) + Ec\epsilon_1(1 + 2C\eta)y(3)^2 +$$
$$\left. + \frac{\epsilon_1 M\,\text{Ec}\,\Pr}{\epsilon_2}\left(y(2)\right)^2\right),$$

with corresponding boundary conditions:

$$y_2(B) = 0, \qquad y_2(0) = 1 + ky_3(0),$$
$$y_4(0) = 1, \qquad y_4(B) = 0.$$

4. Results and discussion

This section investigates the impact of emerging physical parameters on numerically calculated velocity and temperature profiles. It looks into the effects of numerous embedding variables on dimensionless velocity and temperature distributions, such as particle concentration, magnetic parameter (*M*) and Eckert number (*Ec*). The study intends to obtain insight into how these elements impact the flow and thermal behaviour of the system by analysing them. Furthermore, the study investigates the influence of these values on the skin friction coefficient and Nusselt numbers. The data are given in the form of graphs and charts, which provide a visual representation of the results for easier understanding and interpretation.

4.1. Velocity profile

Figures 2 to 6 show how the $f'(\eta)$ gets affected by variation of the volumetric fraction, slip parameter *K*, unsteadiness parameter *S* and magnetic parameter *M*. Figures 2a–2d demonstrate that as the volume fraction value increases, there is also a corresponding increase in velocity.

This phenomenon is attributed to the rise in dynamic viscosity and momentum diffusion. In Figs. 3a–3d, an inverse relationship is observed between the velocity and increasing values of *K*. The reason behind this phenomenon is that an increase in *K* indicates more surface irregularity, which consequently leads to a reduction in velocity at the surface area.
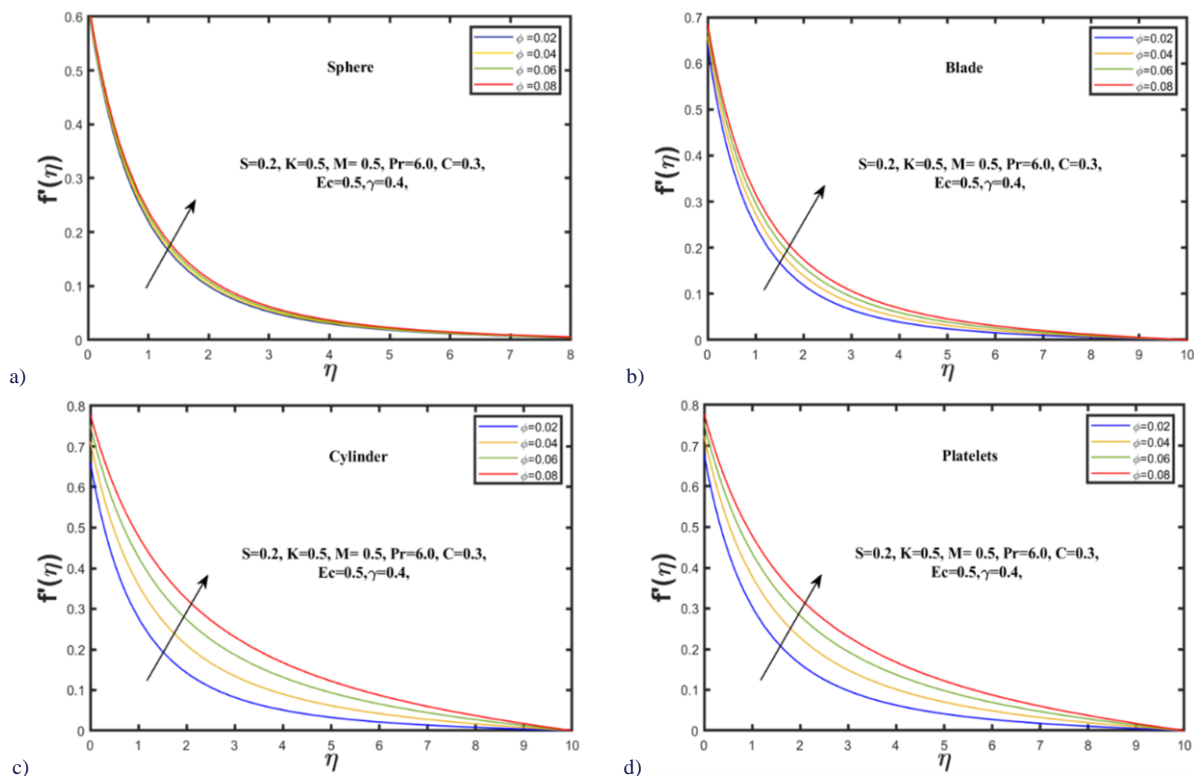
Fig. 2. Impact of ϕ on $f'(\eta)$: a) sphere, b) blade, c) cylinder, d) platelets.
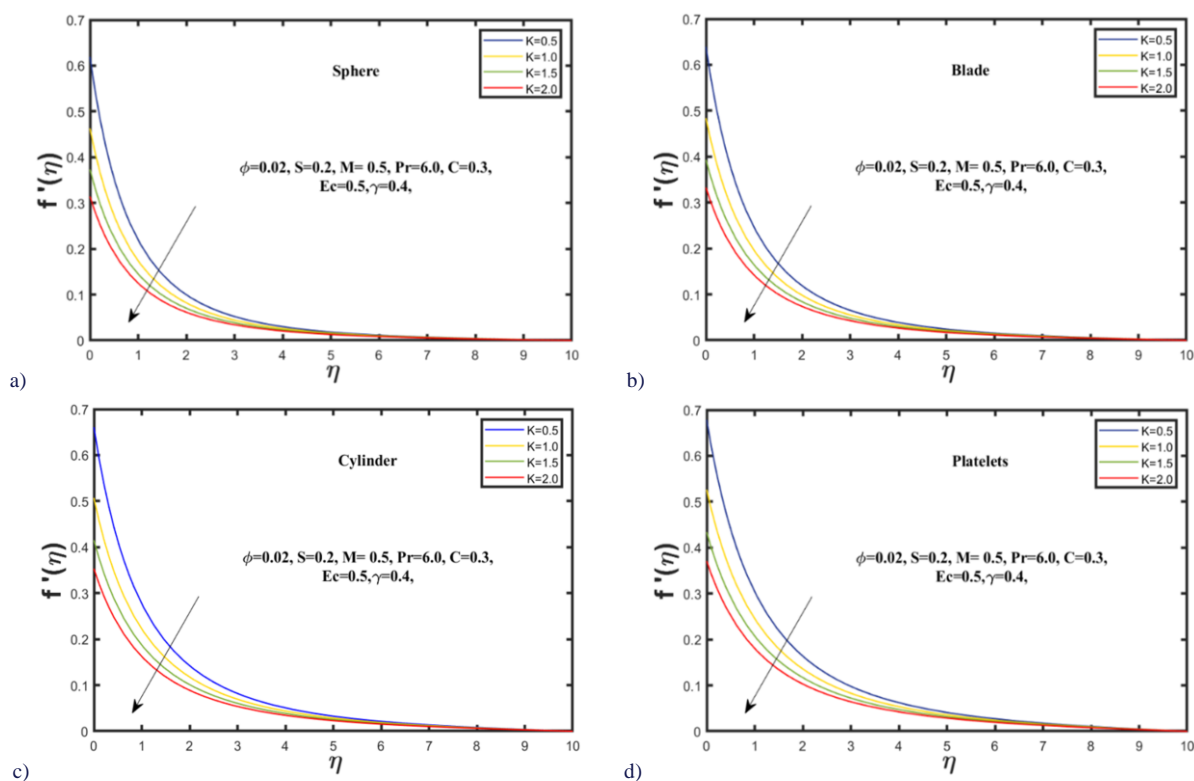
Fig. 3. Impact of K on $f'(\eta)$: a) sphere, b) blade, c) cylinder, d) platelets.

Figures 4a–4d illustrate the relationship between the unsteadiness parameter and velocity. It indicates that the velocity of the nanofluid decreases with an increase in the unsteadiness parameter. This can be attributed to the stretching of the cylinder, which reduces the boundary layer thickness associated with momentum, leading to a decrease in velocity with the unsteady-

ness parameter S.

Figures 5a–5d display the impact of the magnetic parameter on the velocity profile. The results reveal that the velocity decreases with increasing values of M. This phenomenon can be attributed to the rise in Lorentz force, which creates resistive forces between the layers of nanofluid, leading to a reduction in velocity as the magnetic parameter (M) is enhanced.
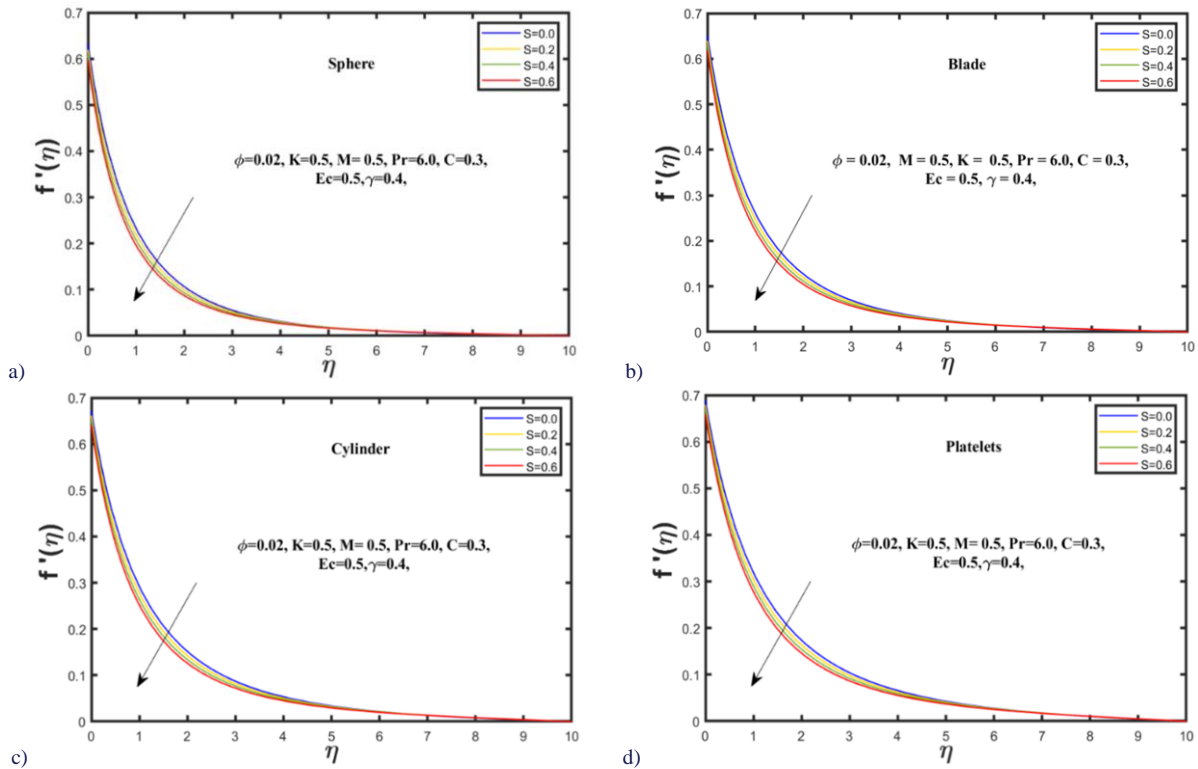
Fig. 4. Impact of S on $f'(\eta)$: a) sphere, b) blade, c) cylinder, d) platelets.
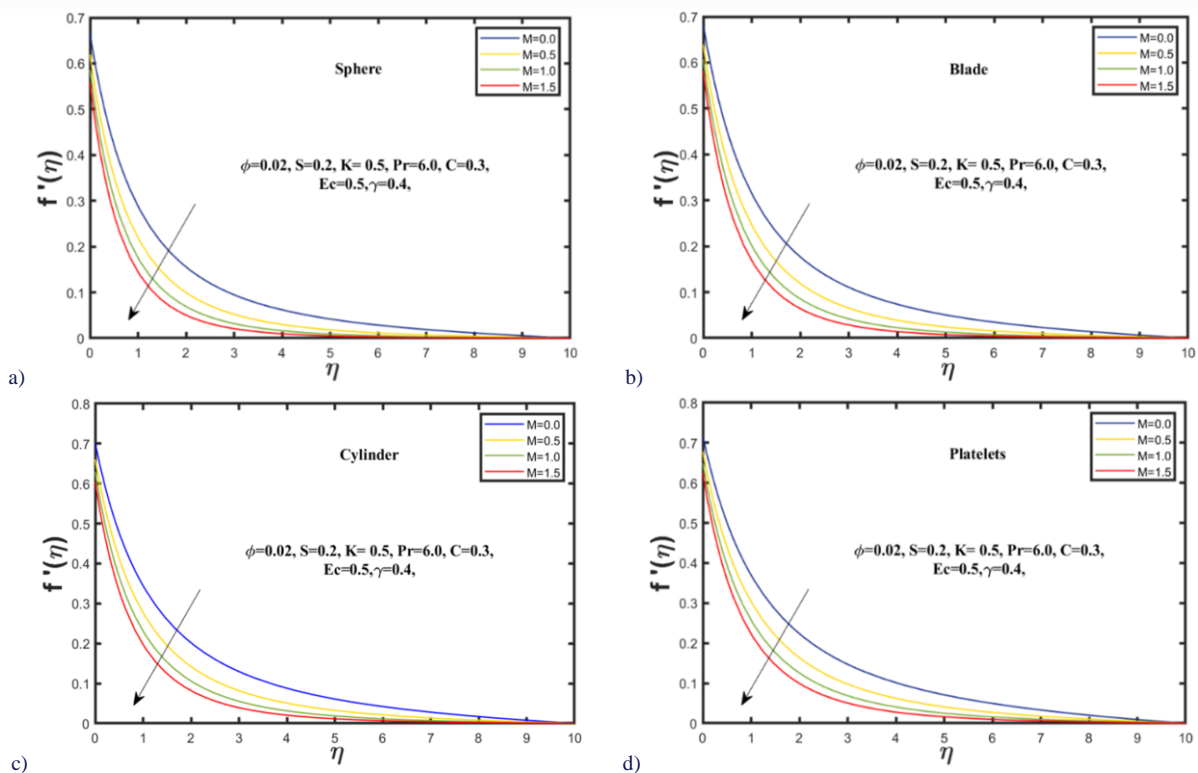
Fig. 5. Impact of M on $f'(\eta)$: a) sphere, b) blade, c) cylinder, d) platelets.

Figure 6 clarifies the influence of each multi-shape nanoparticle on the velocity profile. The study reveals that the SiO_2-H_2O nanofluid attains its maximum velocity with platelet-shaped particles, outperforming cylinder, blade and sphere-shaped particle nanofluids.
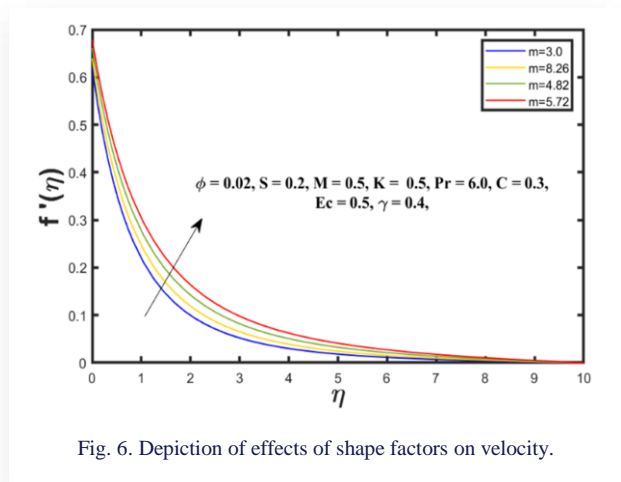
Fig. 6. Depiction of effects of shape factors on velocity.

4.2. Temperature Profile

The effect of volumetric friction on temperature is evident in Figs. 7a–7d. The graph clearly illustrates that an increase in the volumetric fraction value corresponds to a rise in temperature. This phenomenon occurs due to the higher thermal conductivity of the nanoliquid resulting from the increase in volume fraction, leading to higher temperatures.

Figures 8a–8d clearly illustrate that as the value of the unsteadiness parameter S increases, there is a noticeable decrease in the temperature profile. This physical phenomenon arises from the fact that the increase in the unsteadiness parameter enhances heat loss due to cylinder stretching. During the stretching scenario of an unstable flow, the distances between the molecules become larger, leading to a proportional decrease in the temperature profile.

Figures 9a–9d highlight the outcomes of the influence of the magnetic parameter M on the temperature profile. It is observed that the temperature increases with the rising values of the magnetic parameter. This phenomenon occurs because an increase in the values of the magnetic parameter leads to an upsurge in the magnetic field, which opposes fluid movement and consequently causes an increase in the nanofluid temperature.

In Figs. 10a–10d, it is evident that the Prandtl (Pr) number exhibits an inverse relationship with the temperature profile. This phenomenon occurs because the Pr number reduces the thermal diffusivity of the SiO_2-water nanoliquid and decreases the thickness of the thermal boundary layer. Consequently, heat travels more rapidly through the nanoliquid, leading to the observed inverse relationship between the Prandtl number and the temperature profile.

Figures 11a–11d present the relationship between Eckert's (Ec) number and temperature. The graph shows that the temperature increases as the Ec number is increased. This phenomenon occurs because as the Eckert's number increases, there is a corresponding rise in viscous dissipation and kinetic energy. Consequently, the temperature distribution also increases due to the enhanced energy dissipation in the nanofluid.
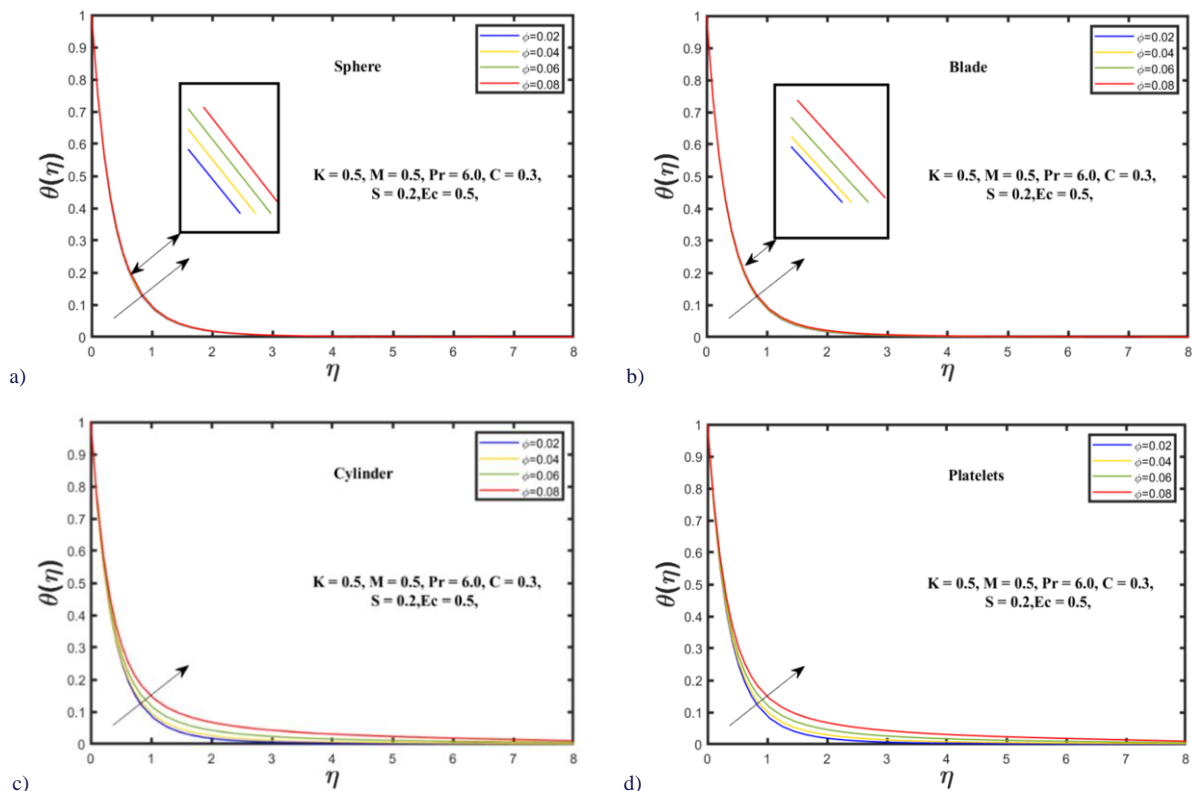
Fig. 7. Impact of volume fraction on $\theta(\eta)$): a) sphere, b) blade, c) cylinder, d) platelets.
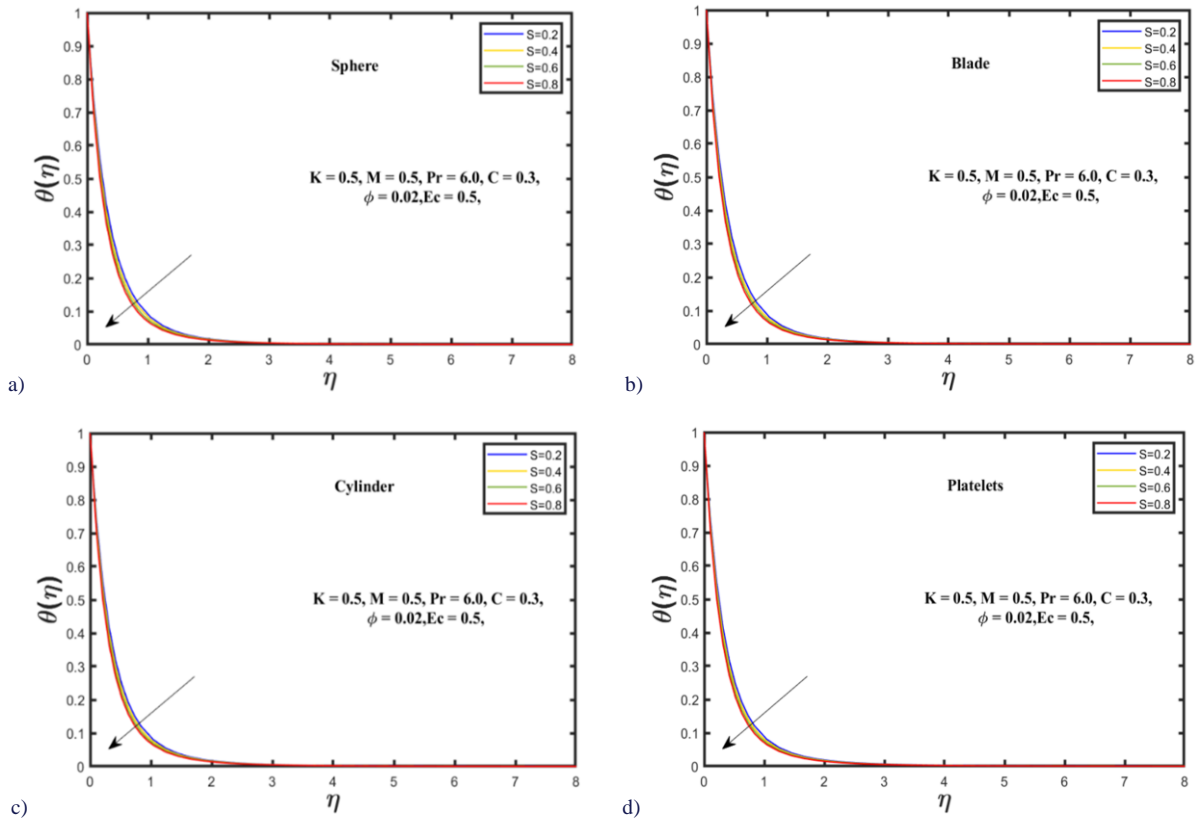
Fig. 8. Effects of S on $\theta(\eta)$): a) sphere, b) blade, c) cylinder, d) platelets.
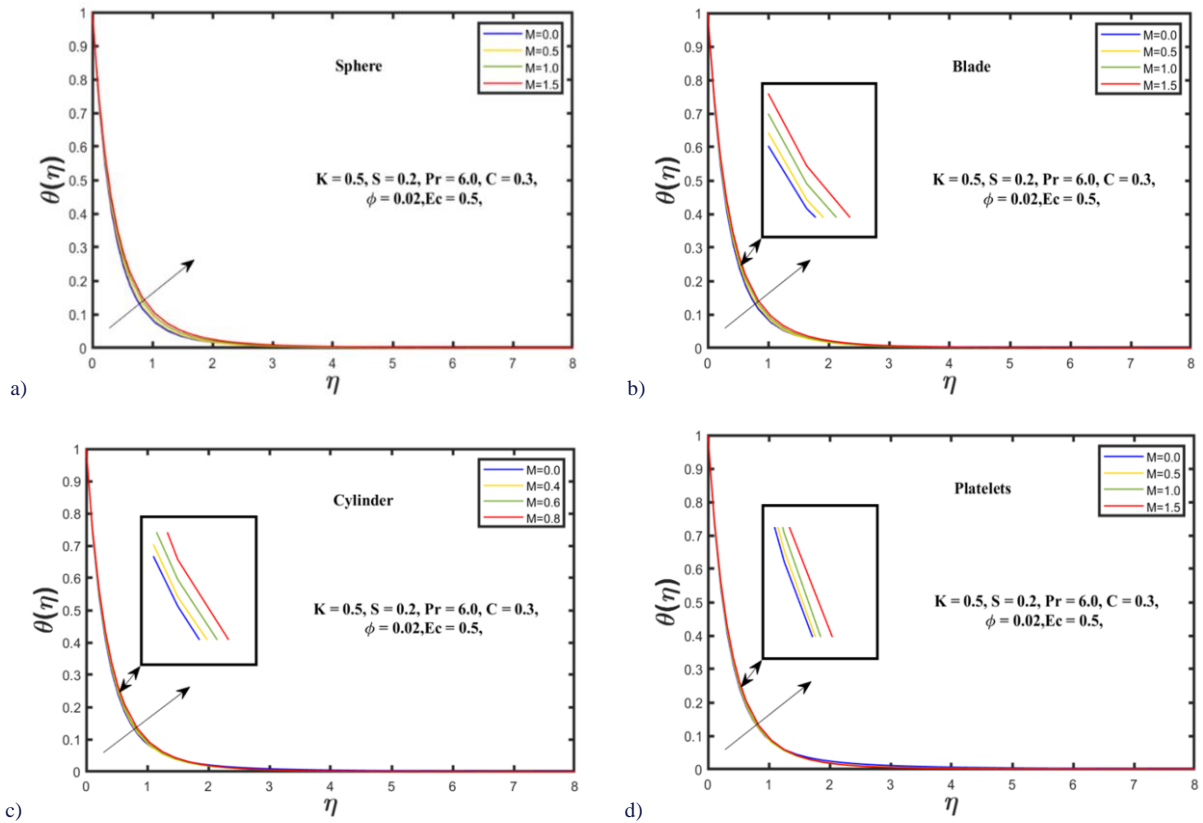
Fig. 9. Effects of M on $\theta(\eta)$): a) sphere, b) blade, c) cylinder, d) platelets.
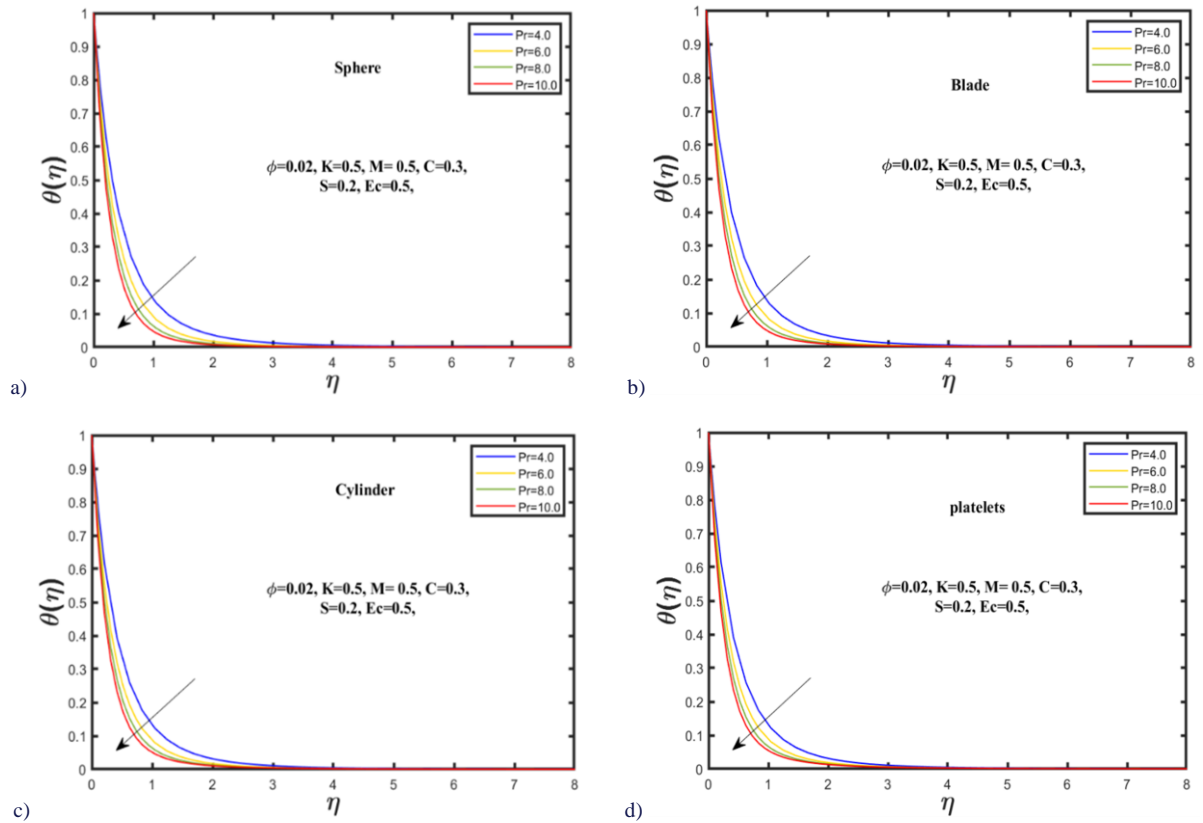
Fig. 10. The effect of Pr on $\theta(\eta)$: a) sphere, b) blade, c) cylinder, d) platelets.
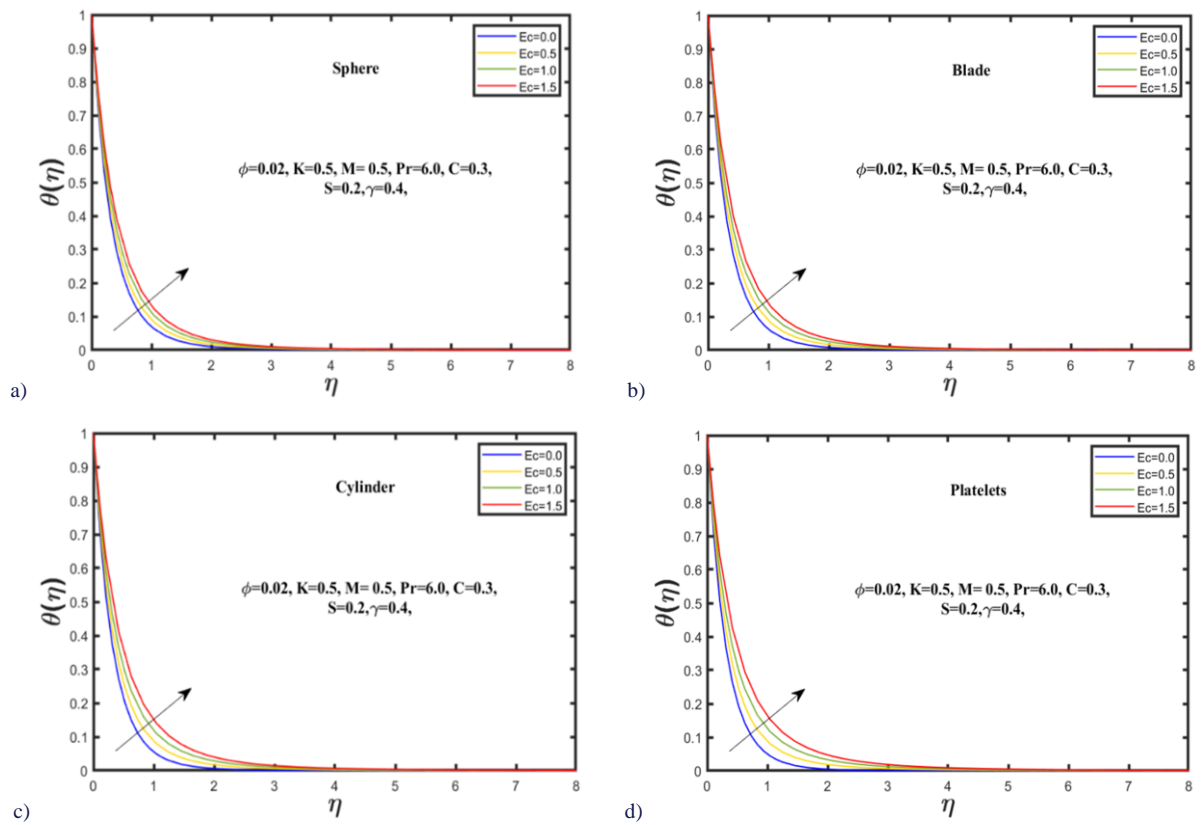
Fig. 11. The effect of Ec on $\theta(\eta)$: a) sphere, b) blade, c) cylinder, d) platelets.

Figure 12 shows the results for the comparison of temperature values for different shape factors $m = 3.0, 8.26, 4.82$ and 5.72, representing sphere, blade, cylinder and platelet shapes, respectively. It is observed that the maximum temperature is noted for platelet and minimum for sphere-shaped nanoparticles of SiO_2.
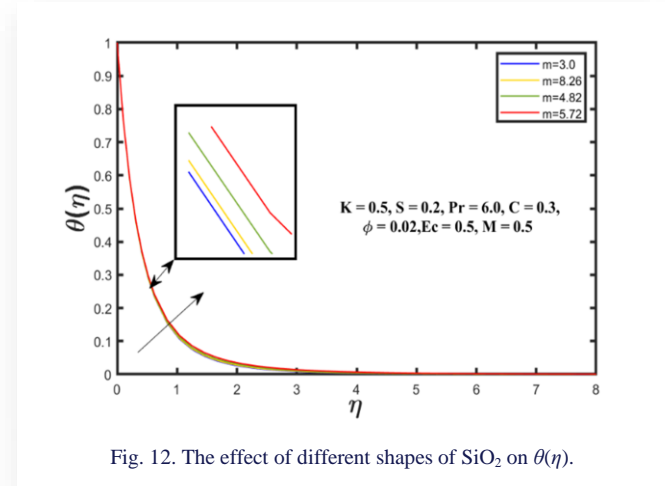
Fig. 12. The effect of different shapes of SiO_2 on $\theta(\eta)$.

4.3. Skin friction and Nusselt number

The study presents numerical values of skin friction in Table 2. It is observed that the skin friction decreases with the slip parameter and increases with the magnetic, volumetric fraction and unsteadiness parameters. Among the different nanoparticle shapes, the platelet shape exhibits both the maximum and minimum values for platelets and sphere-shaped nanoparticles, respectively.

Furthermore, Table 3 illustrates the values of the Nusselt number for variations in the Eckert number, volume percentage, unsteadiness parameter and magnetic parameter. The Nusselt number magnitude decreases with increasing values of M and Ec. Conversely, it increases with higher volumetric percentage and unsteadiness parameter values. Notably, SiO_2 nanoparticles with spherical shapes have the highest Nusselt numbers, while platelet shapes have the lowest values.

5. Conclusions

The study aims to analyze the effects of various parameters on the velocity distribution $f'(\eta)$ and temperature distribution $\theta(\eta)$ in the MHD flow of nanofluids containing different shaped nanoparticles (spherical, platelet, blade and cylinder) in an SiO_2-H_2O nanofluid. The investigations have been focused on understanding how the pertinent parameters impact the velocity and temperature profiles in the system. In conclusion, the velocity profile is positively affected by the volume fraction ϕ, while it is negatively influenced by the slip parameter K, magnetic parameter M and unsteadiness parameter S. The temperature field rises with higher values of volume fraction ϕ, M and Eckert parameter Ec, but decreases with the Prandtl number Pr and unsteadiness parameter S. The skin friction decreases as the slip parameter value increases, but it rises with the magnetic parameter, volume fraction and unsteadiness parameter. The Nusselt number exhibits an increasing trend for increasing values of Pr, ϕ and S, while it decreases with the Eckert number and magnetic parameter.

Acknowledgements

References

[1] Choi, S.U. & Eastman, J.A., (1995). Enhancing thermal conductivity of fluids with nanoparticles. *ASME, 1995 International Mechanical Engineering Congress and Exposition*, 12−17 November, San Francisco, CA, United States.

[2] Talib, S.F.A. Azmi, W.H., Zakaria, I., Mohamed, W., Mamat, A.M.I., Ismail, H., & Daud, W.R.W. (2015). Thermophysical Properties of Silicon Dioxide (SiO2) in Ethylene Glycol/Water Mixture for Proton Exchange Membrane Fuel Cell Cooling Application. *Energy Procedia*, 79, 366–371. doi: 10.1016/j.egypro.2015.11.504

[3] Alsarraf, J., Alnaqi, A.A., & Al-Rashed, A.A.A.A. (2022). Effect of nanoparticles shape on the cooling process of a lithium ion battery in geometry with capillary channels in the presence of phase change material. *Journal of Energy Storage*, 48, 103998. doi: 10.1016/j.est.2022.103998

[4] Akram, J., Akbar, N.S., & Tripathi, D. (2020). Comparative study on ethylene glycol based Ag-Al2O3 and Al2O3 nanofluids flow driven by electroosmotic and peristaltic pumping: a nano-coolant for radiators. *Physica Scripta*, 95(11), 115208. doi: 10.1088/1402-4896/abbd6b

[5] Camara, S., & Sulin, A.B. (2022). Study of a double-acting solar collector for use in the absorption cooling system in hot regions. *Thermal Science and Engineering Progress*, 31, 101286. doi: 10.1016/j.tsep.2022.101286

[6] Abdullatif Alshuhail, L., Shaik, F., & Syam Sundar, L. (2023). Thermal efficiency enhancement of mono and hybrid nanofluids in solar thermal applications – A review. *Alexandria Engineering Journal*, 68, 365−404. doi:10.1016/j.aej.2023.01.043

[7] Ma, M., Xie, M., & Ai, Q. (2022). Simulation on influences of Al2O3 nanofluids as coolant for nuclear power plant based on modified empirical formula of nanofluids thermal properties at high temperature and high pressure. *Energy Sources, Part A: Recovery, Utilization, and Environmental Effects*, 44(1), 454–468. doi: 10.1080/15567036.2022.2046213

[8] Arif, M., Di Persio, L., Kumam, P., Watthayu, W., & Akgül, A. (2023). Heat transfer analysis of fractional model of couple stress Casson tri-hybrid nanofluid using dissimilar shape nanoparticles in blood with biomedical applications. *Scientific Reports*, 13(1), 4596. doi: 10.1038/s41598-022-25127-z

[9] Akram, S., Athar, M., Saeed, K., Razia, A., Muhammad, T., & Ahmed Alghamdi, H. (2023). Mathematical simulation of double diffusion convection on peristaltic pumping of Ellis nanofluid due to induced magnetic field in a non-uniform channel: Applications of magnetic nanoparticles in biomedical engineering. *Journal of Magnetism and Magnetic Materials*, 569, 170408. doi: 10.1016/j.jmmm.2023.170408

[10] Crane, L.J. (1970). Flow past a stretching plate. *Zeitschrift für angewandte Mathematik und Physik*, 21(4), 645−647. doi: 10.1007/BF01587695

[11] Ahmed, J., Shahzad, A., Khan, M., & Ali, R. (2015). A note on convective heat transfer of an MHD Jeffrey fluid over a stretching sheet. *AIP advances*, 5(11), 117117. doi: 10.1063/1.4935571

[12] Hayat, U., Ali, R., Shaiq, S., & Shahzad, A. (2023). A numerical study on thin film flow and heat transfer enhancement for copper nanoparticles dispersed in ethylene glycol. *Reviews on Advanced Materials Science*, 62(1), doi: 10.1515/rams-2022-0320

[13] Yang, H., Haya, U., Shaiq, S., Shahzad, A., Abbas, T., Naeem, M., Khan, S.U., Labidi, T., Kolsi, L., & Zahid, M.A. (2023). Thermal inspection for viscous dissipation slip flow of hybrid nanofluid (TiO$_2$–Al$_2$O$_3$/C$_2$H$_6$O$_2$) using cylinder, platelet and blade shape features. *Scientific Reports*, 13(1), 8316. doi: 10.1038/s41598-023-34640-8

[14] Shaiq, S., Maraj, E.N., & Shahzad, A. (2023). An unsteady instigated induced magnetic field's influence on the axisymmetric stagnation point flow of various shaped copper and silver nanomaterials submerged in ethylene glycol over an unsteady radial stretching sheet. *Numerical Heat Transfer, Part A: Applications*, 85(6), 822−844. doi: 10.1080/10407782.2023.-2193351

[15] Khan, Q., Farooq, M., & Ahmad, S. (2024). Generalized transport analysis on mixed convection squeeze flow of a Casson fluid over an inclined stretching sheet with viscous dissipation and double stratification. *Ain Shams Engineering Journal*, 15(1), 102253. doi: 10.1016/j.asej.2023.102253

[16] Jabeen, K., Mushtaq, M., Mushtaq, T., & Muntazir, R.M.A. (2023). A numerical study of boundary layer flow of Williamson nanofluid in the presence of viscous dissipation, bioconvection, and activation energy. *Numerical Heat Transfer, Part A: Applications*, 85(3), 378−399. doi: 10.1080/10407782.2023.-2187494

[17] Othman, H.A., Ali, B., Jubair, S., Yahya Almusawa, M., & Aldin, S.M. (2023). Numerical simulation of the nanofluid flow consists of gyrotactic microorganism and subject to activation energy across an inclined stretching cylinder. *Scientific Reports*, 13(1), 7719. doi: 10.1038/s41598-023-34886-2

[18] Hayat, U., Shaiq, S., & Shahzad, A. (2023). A Comparative Study of Thin Film Flow of Fe$_3$O$_4$ and Al$_2$O$_3$ Nanoparticles over Stretching Surface Under the Effect of Viscous Dissipation and Magnetohydrodynamics (MHD). Preprint from *Research Square*. doi: 10.21203/rs.3.rs-2693183/v1

[19] Hayat, T., Razaq, A., Khan, S.A., & Alsaedi, A. (2023). Radiative flow of rheological material considering heat generation by stretchable cylinder. *Case Studies in Thermal Engineering*, 44, 102837. doi: 10.1016/j.csite.2023.102837

[20] Khan, W.A., & Pop, I. (2010). Boundary-layer flow of a nanofluid past a stretching sheet. *International Journal of Heat and Mass Transfer*, 53(11), 2477−2483. doi: 10.1016/j.ijheatmass-transfer.2010.01.032

[21] Chen, C.-H. (2004). Combined heat and mass transfer in MHD free convection from a vertical surface with Ohmic heating and viscous dissipation. *International Journal of Engineering Science*, 42(7), 699−713. doi: 10.1016/j.ijengsci.2003.09.002

[22] Cao, J., Cheng, P., & Hong, F. (2009). Applications of electro-hydrodynamics and Joule heating effects in microfluidic chips: A review. *Science in China Series E: Technological Sciences*, 52(12), 3477−3490. doi: 10.1007/s11431-009-0313-z

[23] Hayat, T., Imtiaz, M., & Alsaedi, A. (2016). Melting heat transfer in the MHD flow of Cu–water nanofluid with viscous dissipation and Joule heating. *Advanced Powder Technology,* 27(4), 1301−1308. doi: 10.1016/j.apt.2016.04.024

[24] Maraj, E.N., Faizan, U., & Shaiq, S. (2019). Influence of Joule heating and Partial Slip on Casson Nanofluid Transport Past a Nonlinear Stretching Planar Sheet. *International Conference on Applied and Engineering Mathematics* (pp. 31−36), 27−29 Aug., Taxila, Pakistan. doi: 10.1109/ICAEM.2019.8853731

[25] Khashi'ie, N.S., Arifin, N.M., Pop, I. & Wahid, N.S. (2020). Flow and heat transfer of hybrid nanofluid over a permeable shrinking cylinder with Joule heating: A comparative analysis. *Alexandria Engineering Journal*, 59(3), 1787−1798. doi: 10.1016/j.aej.2020.04.048

[26] Naseem, T., Fatima, U., Munir, M., Shahzad, A., Kausar, N., Nisar, K.S., Saleel, C.A., & Abbas, M. (2022). Joule heating and viscous dissipation effects in hydromagnetized boundary layer flow with variable temperature. *Case Studies in Thermal Engineering*, 35, 102083. doi: 10.1016/j.csite.2022.102083

[27] Rehman, S., Anjum, A., Farooq, M., Hashim, & Malik, M.Y. (2022). Melting heat phenomenon in thermally stratified fluid reservoirs (Powell-Eyring fluid) with joule heating. *International Communications in Heat and Mass Transfer*, 137, 106196. doi: 10.1016/j.icheatmasstransfer.2022.106196

[28] Makhdoum, B.M., Mahmood, Z., Khan, U., Fadhl, B.M., Khan, I., & Eldin, S.M. (2023). Impact of suction with nanoparticles aggregation and joule heating on unsteady MHD stagnation point flow of nanofluids over horizontal cylinder. *Heliyon*, 9(4), e15012. doi: 10.1016/j.heliyon.2023.e15012.

[29] Raza, R., Naz, R., & Abdelsalam, S.I. (2023). Microorganisms swimming through radiative Sutterby nanofluid over stretchable cylinder: Hydrodynamic effect. *Numerical Methods for Partial Differential Equations*, 39(2), 975−994. doi: 10.1002/num.22913

[30] Alsaedi, A., Razaq, A., Hayat, T., & Khan, S.A. (2023). On bioconvective chemically reactive flow involving applications of magnetohydrodynamic and radiation. *Alexandria Engineering Journal*, 75, 549−563. doi: 10.1016/j.aej.2023.06.015

[31] Wazawa T., & Nagai, T. (2023). Joule heating involving ion currents through channel proteins. *Biophysics and Physicobiology*, 20(3), e200030, doi: 10.2142/biophysico.bppb-v20.0030

[32] Manshadi M.K.D., & Beskok, A. (2023). Competing effects of buoyancy-driven and electrothermal flows for Joule heating-induced transport in microchannels. *Flow*, 3, E23. doi: 10.1017/flo.2023.19

[33] Khan, S.A., Eze, C., Lau, K.T., Ali, B., Ahmad, S., Ni, S., & Zhao, J. (2022). Study on the novel suppression of heat transfer deterioration of supercritical water flowing in vertical tube through the suspension of alumina nanoparticles. *International Communications in Heat and Mass Transfer*, 132, 105893. doi: 10.1016/j.icheatmasstransfer.2022.105893

[34] Narayanaswamy, M., Kandasamy, J., & Sivanandam, S. (2022). Go-MoS$_2$/Water Flow over a Shrinking Cylinder with Stefan Blowing, Joule Heating, and Thermal Radiation. *Mathematical and Computational Applications*, 27, 110. doi: 10.3390/mca27060110

[35] Ali, A., Khatoon, R., Ashraf, M., & Awais, M. (2022). Cattaneo–Christov heat flux on MHD flow of hybrid nanofluid across stretched cylinder with radiations and Joule heating effects. *Waves in Random and Complex Media* (pp. 1−18). doi: 10.1080/17455030.2022.2145524

[36] Naseem, T., Shahzad, A., Sohail, M., & Askar, S. (20230). Axisymmetric Flow and Heat Transfer in TiO$_2$/H$_2$O Nanofluid over a Porous Stretching-Sheet with Slip Boundary Conditions via a Reliable Computational Strategy. *Energies*, 16(2), 681. doi: 10.3390/en16020681

[37] Bibi, S., Elahi, Z., & Shahzad, A. (2020). Impacts of different shapes of nanoparticles on SiO$_2$ nanofluid flow and heat transfer in a liquid film over a stretching sheet. *Physica Scripta*, 95(11), 115217. doi: 10.1088/1402-4896/abbc9d